


Mechanical performance analysis in bending of glulam beams reinforced with synthetic Vectran fibres

Análise do desempenho mecânico de vigas de madeira lamelada colada reforçadas com fibras sintéticas de Vectran

Ramon Vilela 
Nilson Tadeu Mascia 
Bruno Fazendeiro Donadon 
Julio Soriano 

Abstract

Synthetic fibres applied as reinforcement in glued laminated timber (glulam) intend to increase the mechanical performance of beams, changing the brittle to ductile mechanical behaviour of wooden beams. This paper investigates the experimental results of glulam beams reinforced with synthetic fibre subjected to bending and compares them with those obtained by both an analytical method and the numerical method using the Ansys® software. Glulam beams were produced with a low-grade strength class wood species (*Pinus elliottii*) glued with an adhesive of emulsion isocyanate polymeric and reinforced with Vectran® synthetic fibres, positioned on the bottom of the beam. This type of fibre is not yet widely used for structural reinforcement. A three-point bending test was performed for loading in the elastic regime of the glulam beams. The results obtained indicate acceptable approximations of vertical displacements and normal stresses due to the bending of the beam with eight layers of synthetic fabric, both favourable to structural safety, in addition to the significant increase in stiffness of glulam with the introduction of Vectran® fibre reinforcement.

Keywords: Glulam. Structural reinforcement. Bending test. Vectran fibres. Finite element method.

Resumo

O uso de fibras sintéticas como reforço em madeira lamelada colada (MLC) tem a finalidade de melhorar o desempenho mecânico de vigas, alterando o mecanismo de ruptura de frágil para dúctil. Este artigo tem por objetivo investigar resultados experimentais de flexão estática de vigas MLC reforçadas com fibras sintéticas e comparar com resultados obtidos tanto por método analítico quanto por numérico com o auxílio do software Ansys®. As vigas de MLC foram produzidas com Pinus elliottii, uma espécie de madeira de baixa resistência, colada com adesivos de emulsão polimérica de isocianato (EPI) e reforçadas com tecido de fibras sintéticas de Vectran® posicionado na face inferior da viga. Este tipo de fibra ainda não é largamente utilizado para reforço estrutural. Foi realizado ensaio de flexão a três pontos com carregamento no regime elástico das vigas de MLC. Os resultados obtidos mostram aproximações aceitáveis do deslocamento vertical e tensões normais devido à flexão da viga com reforço de oito camadas de tecido sintético, ambos a favor da segurança, além do expressivo aumento de rigidez da viga ao se introduzir o reforço de fibras de Vectran®.

Palavras-chave: MLC. Reforço estrutural. Ensaio de flexão. Fibras de Vectran. Método dos elementos finitos.

¹Ramon Vilela
¹Universidade Estadual de Campinas
Campinas - SP - Brasil

²Nilson Tadeu Mascia
²Universidade Estadual de Campinas
Campinas - SP - Brasil

³Bruno Fazendeiro Donadon
³Universidade Estadual de Campinas
Campinas - SP - Brasil

⁴Julio Soriano
⁴Universidade Estadual de Campinas
Campinas - SP - Brasil

Recebido em 13/02/23
Aceito em 05/06/23

Introduction

The development of wood engineering technology significantly increased in the nineteenth century when Friedrich Otto Hetzer patented glued laminated timber (glulam), a structural piece comprising two or more wood laminations glued with waterproof adhesive that results in a high strength-to-weight ratio (ONG, 2015).

Glulam can be considered the evolution of lumber beams as the production process involves a more advanced technique, which distributes the natural defects of the wood more evenly in the piece, reducing the standard deviation of its physical and mechanical properties, and therefore increasing its bending strength (THORHALLSSON; HINRIKSSON; SNÆBJÖRNSSON, 2017). The laminations with their grains oriented along the length of the piece can be distributed in the cross-section to generate homogeneous or combined glulam, and in turn, straight, tapered, or curved pieces can be manufactured (BRITISH..., 1999; GAO *et al.*, 2019).

Glulam elements also show significant potential for structural and architectural applications, as supported by numerous studies highlighting their differentials and excellent performances in theoretical, experimental, and numerical analyses (FIORELLI; DIAS, 2011; TIMBOLMAS *et al.*, 2021).

Even with glulam showing improvement in some characteristics when compared with solid-sawn lumber, research on reinforcement has aimed at investigating the mechanical performance, focusing on the increase in stiffness and strength of low-grade glulam. According to Raftery and Kelly (2015), these findings show that reinforcement can contribute to the bending strength, decrease the standard deviation of the characteristic bending strength, and change the failure mode from brittle (tensioned region) to ductile rupture (compressed region).

Furthermore, the reinforcement arrangement in the beam is an important factor to consider, which can be applied internally or to edge faces of the cross-section (ŚLIWA-WIECZOREK *et al.*, 2021) by surface groove seal, glued between the laminations, or by external bonding, each of which is used with different structural purposes.

Among the materials used for reinforcement in glulam beams, metallic and fibrous materials stand out. The first type shows high mechanical properties using steel bars and steel plates (PEIXOTO *et al.*, 2021; WANG *et al.*, 2021). In the second type of reinforcement materials, natural fibres of sisal and flax can be mentioned, which can be grown in abundance and with low processing costs (BORRI; CORRADI; SPERANZINI, 2013). Synthetic fibres have the most diverse advantages of industrially produced materials as they are stable and can achieve high mechanical properties with thin fabrics. In the field of synthetic fibres, findings show the feasibility of using carbon fibre-reinforced polymers (RESCALVO *et al.*, 2021; VAHEDIAN; SHRESTHA; CREWS, 2019) and glass fibre-reinforced polymers (SHAHIDUL ISLAM; SHAHNEWAZ; ALAM, 2021). Given the importance of using synthetic fibres to reinforce glulam beams and the challenge of seeking new materials, an experimental study used the Vectran[®] fibre-reinforced polymer composite (DONADON *et al.*, 2020).

Considering the various options for reinforcing glulam beams to extrapolate the limits found in the tests and to give greater freedom in creating projects, computational modelling is an allied technology for innovations in this field of structural engineering. Uzel *et al.* (2018) evaluated the behaviour of glulam beams reinforced with fibreglass, steel, and aluminium nets, which were glued between two laminations. These researchers used Ansys software, with wood laminations represented by solid elements (SOLID45) and the bonding surfaces of the laminations modelled by contact and target pairs (CONTA174, TARGE170), which resulted in higher rigidity than the experimental results and with mean value differences of 14%. İşleyen *et al.* (2021) performed a finite element simulation with ABAQUS software to evaluate the behaviour of glulam beams reinforced with CFRP with wood laminations discretized by an 8-node hexahedron element (C3D8R) and adopted linear elastic-perfectly plastic and linear-elastic models in compression and tension, respectively. The CFRP was discretized by 4-node elements (S4R) using the linear elastic model, and its contact with the laminations was perfectly adopted.

Some analytical or numerical methods can be used to analyse and design reinforced glulam beams. This work involved an experimental procedure where glulam beams reinforced with synthetic Vectran[®] fibre were subjected to bending. The results were then evaluated using both the analytical model of the transformed section method and numerical analysis by the finite element method (FEM) using the ANSYS[®] Workbench software.

Materials and methods

Materials

To achieve the objectives of this research, the experimental procedures were conducted in three steps: first, wood boards were classified and selected to produce the glulam beams; second, unreinforced glulam beams were characterized; and finally, beams reinforced with Vectran[®] synthetic fibres glued with emulsion polymer isocyanate (EPI) were experimentally tested.

The wood species used in this study was *Pinus elliottii* sourced from reforestation, and its origin in Brazil was not provided by the supplier. The wood boards were dried to less than 12% and classified by density. The denser boards were used for the external layers, while the less dense ones were utilised for the internal layers.

From this, three prototype glulam beams were produced, each with a length of 3000 mm and comprising nine softwood laminations, each 20 mm thick. The cross-section of each glulam beam totalled 180 mm in height and 53 mm in width.

Table 1 shows the physical and mechanical properties of each analysed beam. The numbers assigned to beams RG4, RG6, and RG8 are associated with the number of layers of reinforcement applied in the 2nd step of the experimental procedure.

The fabric used as reinforcement was produced from Vectran[®] fibres obtained from the melt spinning of a liquid crystal polymer (LCP) (KURARAY, 2022). This product has not been used for reinforcement purposes thus far but represents a successful application in other engineering areas, such as aerospace and military areas, safety materials and protective apparel, and industrial applications such as cables and composites. The density of the fibre is 1400 kg/m³, its longitudinal modulus of elasticity is 50.16 GPa, and the tensile strength is 2850 MPa (DONADON *et al.*, 2020). The reinforcements were applied to the bottom of the beam in the tension stress region.

The adhesive used to glue the layers of fibre reinforcement to the bottom of the glulam beams was the bicomponent of emulsion polymer isocyanate (EPI) produced from ReactITE EP-925 and Hardener 200. The first component is a polyvinyl acetate emulsion adhesive and its reagent is a polymeric MDI. The product has a density of 1280 kg/m³ and a longitudinal modulus of elasticity of 4 GPa (FRANKLIN..., 2022).

To determine the physical properties of the reinforcement, the volume theory for composites was used to calculate the specific volume of fibre (V_f), according to Equation 1 (CAMPBELL, 2010).

$$V_f = \frac{W_f/\rho_f}{W_f/\rho_f + W_a/\rho_a} \quad \text{Eq. 1}$$

Where:

V is the volume;

f and a are the fibre and adhesive indexes, respectively; and

W and ρ are the mass and specific mass, respectively.

The specific volume of adhesive can be determined considering a 5% void volume, according to Huang and Talreja (2005). Thus, Equation 2 provides the parameter required for reinforcement.

Table 1 - Density and elastic properties of glulam beams*

Beam	Density (kg/m ³)	EL (MPa)	ET (MPa)	ER (MPa)	GLT (MPa)	GLR (MPa)	GTR (MPa)
RG4	664.4	11,783.0	589.2	981.9	790.8	841.7	84.2
RG6	605.1	13,752.5	687.6	1,146.0	923.0	982.3	98.2
RG8	520.8	8,841.1	442.1	736.8	593.4	631.5	63.2
Mean	596.8	11,458.9	572.9	954.9	769.1	818.5	81.9
Std. D.	72.16	2,471.70	123.58	205.97	165.89	176.55	17.65
C.V. (%)	12.09	21.57	21.57	21.57	21.57	21.57	21.57

Note: *the subscript indexes represent the wood's orthotropic directions: L for longitudinal (parallel to grain), T for tangential, and R for radial.

$$X_c = X_f V_f + X_a V_a \quad \text{Eq. 2}$$

Where X is the parameter to be determined, such as the longitudinal modulus of elasticity (E_c) or specific mass (ρ_c).

Table 2 presents the specifications of the reinforcement applied in each beam.

Experimental bending tests

Characterization of the glulam beams

Pinus elliottii was used, and the modulus of elasticity (MOE) was obtained by a three-point bending test. The MOE parallel to the grain is determined from the vertical displacement considering the effects of bending and shear, according to Equation 3.

$$\delta = \frac{Pl^3}{48EI} + \frac{\kappa Pl}{4GA} \quad \text{Eq. 3}$$

Where:

δ represents the difference between the displacements corresponding to 50% and 10% of the maximum applied load;

P the difference between the loads at 50% and 10% of the maximum load;

l the span;

E ($= E_L$) the MOE parallel to grain;

I the cross-sectional moment of inertia of the beam;

A the cross-sectional area; G the shear modulus; and

κ the shape factor.

Considering the shape factor for rectangular sections $\kappa = 1.2$ and adopting the correlation $G = E/14$ (GAGNON; PIRVU, 2011), the modulus of elasticity is written as Equation 4.

$$E = \frac{P}{\delta} \left(\frac{l^3}{48I} + \frac{21l}{5A} \right) \quad \text{Eq. 4}$$

Thus, the modulus of elasticity was obtained experimentally, according to NBR 7190 (ABNT, 1997), and the other elastic constants were determined from the correlations established by Bodig and Jayne (1993) and Mascia and Vanalli (2012) for softwood species.

Reinforcement glulam beams

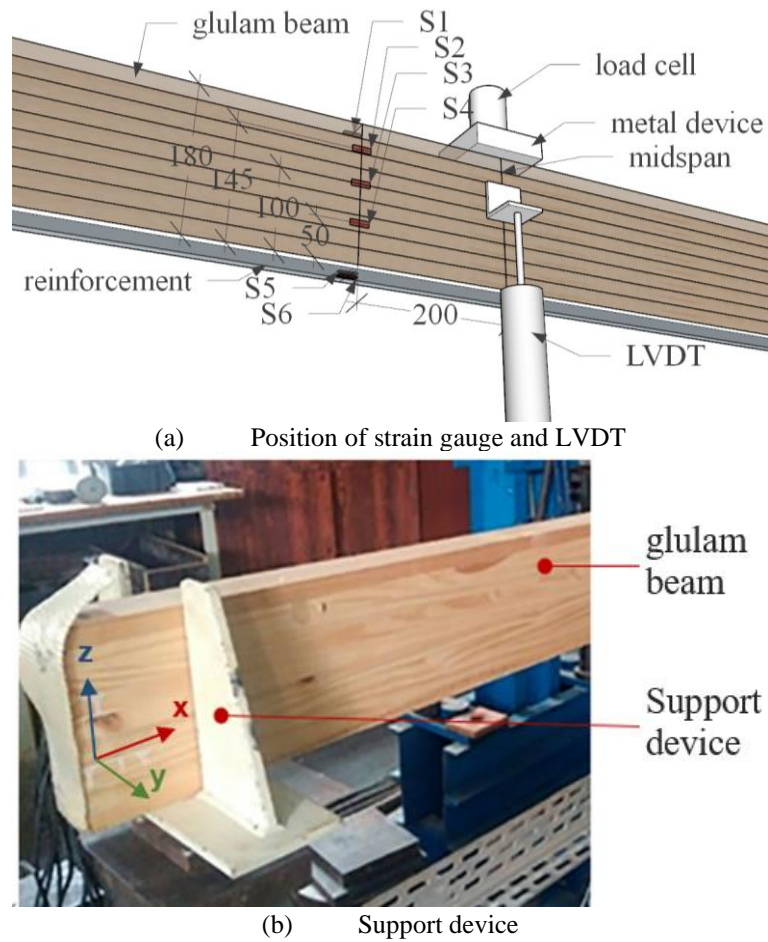
The three-point bending test was conducted to obtain the displacements and the normal stress of the Glulam beam reinforced with synthetic fibre to compare it with the analytical and numerical results. Figure 1 shows the equipment used in the bending test, including the distributed load in a length of 100 mm, five strain gauges used 200 mm apart from the beam centre, and one transducer (LVDT). To avoid possible errors due to physical or geometric eccentricities around the beam axes, the supports were increased with a metal device that restricted the displacements in the y -axis and the rotation around the beam's longitudinal axis.

The data of the transducers and the load cell and strain gauge were collected by a data acquisition system and tabulated as a function of time. The sampling rate was 1 second. The load application device consisted of an open frame anchored at four points with a capacity of 300 kN and a load cell with a capacity of 150 kN. The load was applied by a hydraulic jack with a pump.

Table 2 - Elastic properties of Glulam beams*

Beam	Number of layers	Thickness reinforcement (mm)	Fibre mass (kg)	Adhesive mass (kg)	ρ_c (kg/m ³)	E_c (MPa)
RG4	4	3.0	0.88	0.87	841.65	84,170
RG6	6	6.0	1.32	1.20	982.32	98,232
RG8	8	9.0	1.76	1.42	631.51	63,151

Figure 1 - Strain gauge, transducers, and support of the beams



The first step of the test was to characterize the longitudinal modulus of elasticity of the glulam beam, where a load of approximately half of its ultimate load was applied. This load was estimated from a previous test. At this stage, the beam was only equipped with the transducer T1, which allowed the measurement of vertical displacements in the midspan of the beams. The transducer resolution was set as 4 μm .

Analytical method

Calculating the normal stresses in a specific strain gauge is possible by applying the relationship between stress σ and strain ε , according to Equation 5.

$$\sigma = E\varepsilon \tag{Eq. 5}$$

Where:

σ is the estimated stress;

E is Young's modulus according to the characterization of the beams (Table 1); and

ε is the strain.

By the equilibrium of forces, Equation 6 gives the bending moment acting at the position of strain gauge.

$$M(x) = \frac{Px}{2} \tag{Eq. 6}$$

Where:

M is the bending moment;

P is the load applied at the midspan; and

x is the distance in the x -axis between the strain gauge and nearest support.

To determine the effective bending stiffness EI_{ef} of the reinforced beam, the transformed section is employed where the fibre width is multiplied by η , defined by Equation 7.

$$\eta = \frac{E_f}{E_{w,0}} \quad \text{Eq. 7}$$

Where:

η is the transformation factor of the fibre section width;

E_f is the modulus of elasticity of the fibre; and

$E_{w,0}$ is the longitudinal modulus of elasticity of the wood.

Equation 8 determines the centroid in the z -axis.

$$z_{CG} = \frac{b_w h_w \bar{z}_w + \eta b_f h_f \bar{z}_f}{A_w + \eta A_f} \quad \text{Eq. 8}$$

Where:

z_{CG} is the centroid of the overall section;

b is the width;

h is the height \bar{z} distance on the z -axis of the centroid of the section and the origin;

A is the cross-sectional area; and

w and f are the indexes for wood and fibre, respectively.

Thus, Equation 9 determines the effective bending stiffness EI_{ef} as follows:

$$EI_{ef} = E_w \left(\frac{b_w h_w^3}{12} + A_w d_w^2 \right) + \eta E_w \left(\frac{b_f h_f^3}{12} + A_f d_f^2 \right) \quad \text{Eq. 9}$$

Where d_w and d_f are the distances between the centroid of the total section z_{CG} and the centroid of each section (z_w and z_f), respectively.

To obtain a better fit of the results, the displacements due to the shear effect were considered. Thus, Equation 10 shows how to determine the effective shear stiffness GA_{ef} for a transformed section method (GAGNON; PIRVU, 2011).

$$GA_{ef} = \frac{e^2}{\left(\frac{h_1}{2G_1 b_1} \right) + \left(\sum_{i=1}^{n-1} \frac{h_i}{G_i b_i} \right) + \left(\frac{h_n}{2G_n b_n} \right)} \quad \text{Eq. 10}$$

Where e is the distance between the centres of gravity of the upper and lower layers;

h_1 is the stiffness of the i -layer;

G_i is the shear modulus of the i -layer;

b_i is the width of the i -layer; and

n is the last layer.

However, Equation 11 determines the normal stresses σ_i at a given point in a section due to bending.

$$\sigma_w(z) = E_w \frac{M}{EI_{ef}} z; \sigma_f(z) = \eta E_w \frac{M}{EI_{ef}} z \quad \text{Eq. 11}$$

Where z is the location in the z -axis of the analysed point.

For the numerical and analytical models, the fibre-adhesive composite was assumed to be an elastic isotropic material with Poisson's ratio $\nu = 0.3$. The orthotropic material model was used for wood, and Table 3 shows the elastic correlations necessary to develop the analyses.

Numerical analysis

In the ANSYS® simulation, the contact between all elements was considered bonded, therefore without relative displacement between them. The numerical model was discretized using the maximum element size

of 10 mm, generating a mesh containing 34,260 SOLID185, 32,562 CONTA174, 32,562 TARGE170, and 30 SURF154 elements. This mesh configuration was used for the three simulated beams (ANSYS, 2018).

SOLID185 is a solid element used to model 3-D structures. This element comprises eight nodes with three degrees of freedom at each node, translated in the x , y , and z -directions (Figure 2). The element has elastic, plasticity, hyperelasticity, creep, stress stiffening, large deflection, and large strain capabilities. This element was applied to simulate glulam beams.

TARGE170 is used to represent several 3-D target surfaces. In this model, the element was used to simulate the reinforcement at the bottom of the beam composed of Vectran® fibres.

CONTA174 was used in the model to represent contact between 3-D target surfaces and a deformable surface defined by this element (i.e., reinforcement to glulam beam).

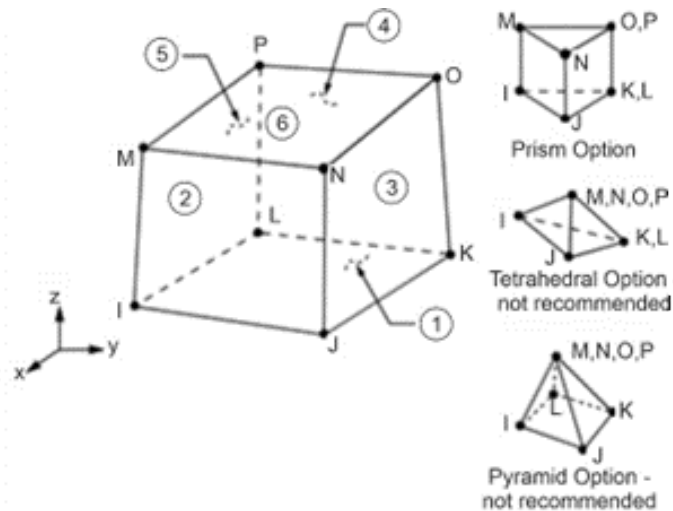
The load was applied on the element SURF154. The element comprises eight nodes and material properties. Figure 3 shows how duplicated triangular elements are used to form the element. Loading is carried out in the numerical model by 10 steps of equal 1.08 kN increments.

Table 3 - Correlations and Poisson's ratios for Pinus (BODIG; JAYNE, 1993)

Description	Correlations		
Long modulus of elasticity	$E_L/E_L = 1.00$	$E_L/E_T = 20.00$	$E_R/E_L = 12.50$
Shear modulus	$E_L/G_{LR} = 14.00$	$E_L/G_{LT} = 14.90$	$E_L/G_{RT} = 140.00$
Poisson's ratio	$\nu_{LR} = 0.37$	$\nu_{LT} = 0.42$	$\nu_{TR} = 0.45$

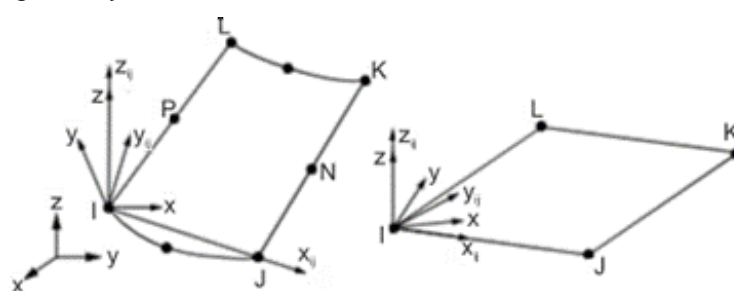
Note: *the subscript indexes represent the wood's orthotropic directions: L to longitudinal (parallel to grain), R to radial, and T to tangential.

Figure 2 - SOLID185 homogeneous structural solid geometry



Source: Ansys (2018).

Figure 3 - SURF154 geometry



Source: Ansys (2018).

Figure 4 shows the mesh discretization and boundary conditions of the numerical model simulated by ANSYS®.

Results and discussion

Vertical displacement

Figure 5 depicts the displacement results at the midspan of the RG8 beam for both nonreinforced and reinforced beams with eight layers of fibre cases, as obtained from experimental, analytical, and numerical methods. The experimental results of the nonreinforced beam show a deviation in the load level of approximately 2.00 kN, with a change in the inclination of the curve, indicating a reduction in stiffness. This behaviour was not observed in the experimental reinforced beam, which showed a more linear behaviour and a higher stiffness than the nonreinforced beam.

Table 4 presents a comparison of the displacement results of reinforced beams obtained through experimental, analytical, and numerical methods to RG8. The initial nonregular displacements of the experimental results were observed up to 2.02 kN. The numerical and analytical results show a linear pattern and a constant difference of 2.53% between them, demonstrating that the methods produce different results; however, they are very similar to each other.

Figure 6 shows the displacement results at the midspan of the RG6 beam. The nonreinforcement beam experimentally presented slightly more stiffness than the reinforced beam until approximately 6 kN; however, after this load level, the reinforced beam showed a higher stiffness.

Figure 4 - 3D modelling simulated by ANSYS®

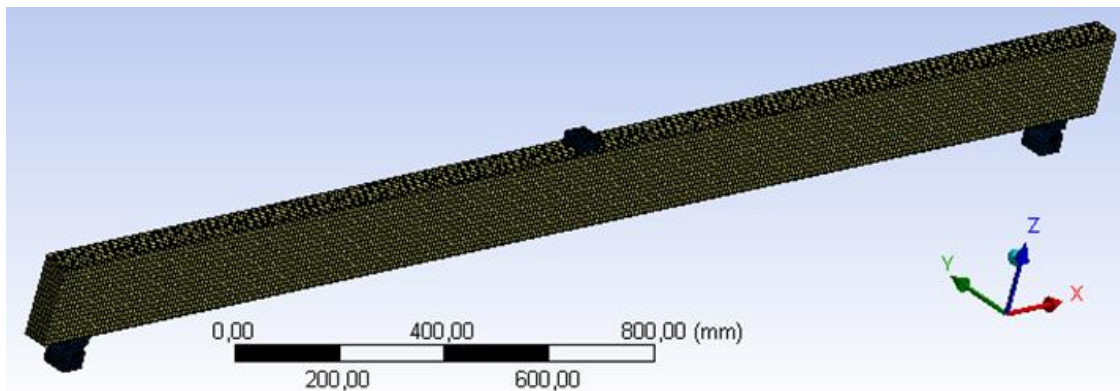


Figure 5 - Vertical displacements at the midspan of the RG8 beam

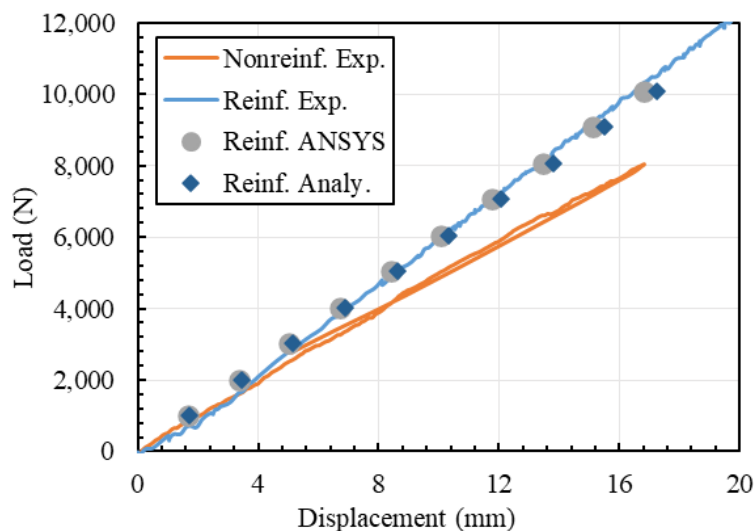
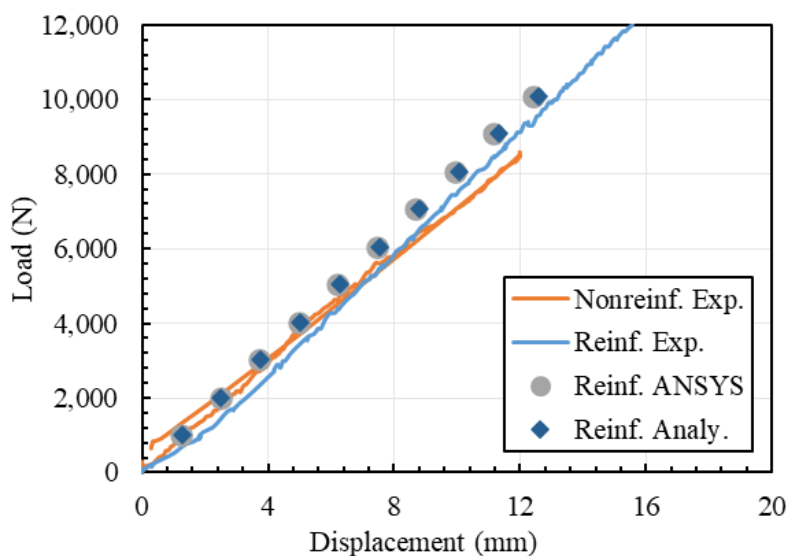


Table 4 - Comparison among the vertical displacements of RG8

Load (kN)	Vertical displacement (mm)			Difference (%)		
	Analytic	ANSYS	Experimental	Analytic/Experimental	ANSYS/Experimental	Analytic/Numeric
1.01	1.72	1.68	2.35	-26.78	-28.63	-2.53
2.02	3.45	3.36	3.92	-12.05	-14.28	-2.53
3.02	5.17	5.04	5.47	-5.40	-7.79	-2.53
4.03	6.90	6.72	7.02	-1.79	-4.27	-2.53
5.04	8.62	8.40	8.64	-0.21	-2.73	-2.53
6.05	10.34	10.08	10.18	1.57	-1.00	-2.53
7.06	12.07	11.76	11.72	2.94	0.34	-2.53
8.06	13.79	13.44	13.40	2.94	0.33	-2.53

Figure 6 - Vertical displacements at the midspan of the RG6 beam



A comparison of the vertical displacement results for reinforced beams obtained by experimental, analytical, and numerical methods for RG6 is shown in Table 5. Initially, the experimental results showed nonregular displacements up to a load of 2.02 kN. As the load increased, the simulated methods more adequately represented the experimental results. The numerical and analytical results had a mean difference of 1.43%, indicating a negligible difference between these methods.

Figure 7 displays the results of the displacements at the middle span of the RG4 beam. The nonreinforcement beam presents a linear behaviour, whereas the reinforced beam experimentally shows a significant deflection point close to the 2.00 kN load, showing evidence of more rigidity than the nonreinforcement beam until the load level of 7.00 kN. In this case, the numerical and analytical results were closer to the nonreinforced beam than to the reinforced beam due to the nonlinear behaviour of the reinforced beam.

Table 6 presents a comparison of the vertical displacement results for RG4, which were obtained using experimental, analytical, and numerical methods. As with the previous comparisons, nonlinearity was observed in the initial loads, as observed by the difference between the linear methods and the experimental results. The numerical and analytical methods had a mean difference of 2.05%, indicating a slight discrepancy between them.

Finally, a comparison of displacements between loads of 2.00 kN and 8.00 kN was performed to observe the stiffness differences between the reinforced and nonreinforced beams, and Table 7 presents the results. This range of loads was selected to avoid initial nonlinear behaviour. The comparison reveals that the addition of reinforcement significantly reduces the beam displacement by an average of 21.3%. Furthermore, Table 7 highlights that RG8 exhibits the most improvement in stiffness compared to its nonreinforced specimen, followed by the RG4 and RG6 beams.

Table 5 - Comparison among the vertical displacements of RG6

Load (kN)	Vertical displacements (mm)			Differences (%)		
	Analytic	ANSYS	Experimental	Analytic/Experimental	ANSYS/Experimental	Analytic/Numeric
1.01	1.26	1.24	1.94	-35.18	-36.11	-1.44
2.02	2.52	2.48	3.30	-23.84	-24.93	-1.43
3.02	3.77	3.72	4.58	-17.66	-18.84	-1.43
4.03	5.03	4.96	5.82	-13.55	-14.79	-1.43
5.04	6.29	6.20	7.05	-10.74	-12.02	-1.43
6.05	7.55	7.44	8.25	-8.51	-9.83	-1.43
7.06	8.81	8.68	9.49	-7.25	-8.58	-1.43
8.06	10.06	9.92	10.74	-6.33	-7.67	-1.43

Figure 7 - Vertical displacements at the midspan of the RG4 beam

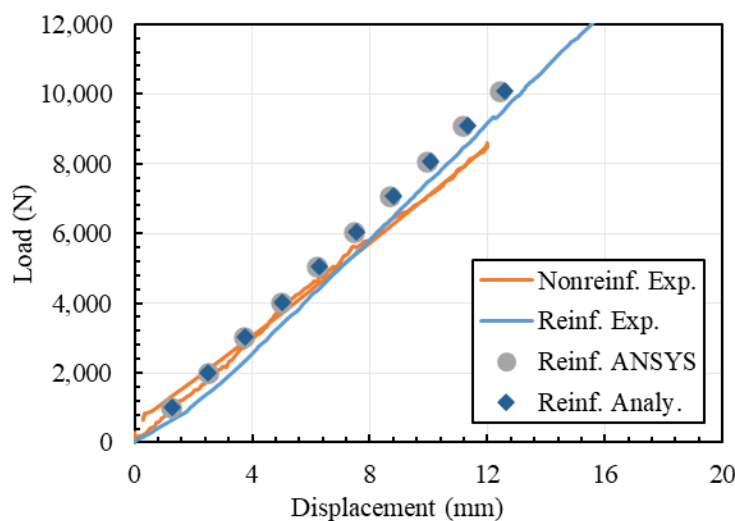


Table 6 - Comparison among the vertical displacements of RG4

Load (kN)	Vertical displacement (mm)			Difference (%)		
	Analytic	ANSYS	Experimental	Analytic/Experimental	ANSYS/Experimental	Analytic/Numeric
1.01	1.54	1.50	2.27	-32.42	-33.80	-2.05
2.02	3.07	3.01	3.86	-20.50	-22.13	-2.05
3.02	4.61	4.51	5.38	-14.26	-16.01	-2.05
4.03	6.15	6.02	6.80	-9.69	-11.54	-2.05
5.04	7.68	7.52	8.15	-5.77	-7.70	-2.05
6.05	9.22	9.03	9.42	-2.13	-4.14	-2.05
7.06	10.75	10.53	10.60	1.42	-0.66	-2.05
8.06	12.29	12.04	11.71	4.98	2.83	-2.05

Table 7 - Comparison between displacements of nonreinforced and reinforced beams

Beam	Nonreinforced (mm)			Reinforced (mm)			Difference (%)
	P (kN) 2.00	P (kN) 8.00	Diff. (%)	P (kN) 2.00	P (kN) 8.00	Diff. (%)	
VG8	4.14	16.77	12.63	3.92	13.28	9.36	-25.86
VG6	2.76	11.32	8.56	3.41	10.67	7.25	-15.24
VG4	3.02	12.44	9.42	4.52	11.80	7.28	-22.72
Mean	3.31	13.51	10.20	3.95	11.92	7.97	-21.28
Std. Dev.	0.60	2.35	1.75	0.45	1.07	0.99	4.45
COV. (%)	18.06	17.38	17.16	11.43	8.99	12.39	20.94

Normal stress

Figure 8 depicts the normal stress measured and calculated for the RG8 beam at the strain gauge position under a load of 10.08 kN. The experimental results demonstrate nonlinear behaviour, indicating that the layers have variations in the values of their elastic characteristics, as seen in Section 2.1 of this article. The analytical and numerical results reveal acceptable convergence at the top and bottom of the cross-section, where the stresses are critical. Taking into account the experimental and analytical procedures, the differences at the top were 1.3%, and those at the bottom were 25.5%. Considering the experimental and numerical results, the stress differences were 12.7% and 10.1% at the top and bottom, respectively. These differences are in favour of structural security.

Figure 9 shows the normal stresses of the analytical and numerical results in the strain gauge positions of the RG6 beam to a load of 10.08 kN. The inclinations of the analytical and numerical stress paths are parallel to each other but differ significantly from the experimental results. This may indicate that stiffness, and consequently, the longitudinal modulus of elasticity of the analytical and numerical models, is different from that of the experimental model.

Considering both the experimental and analytical procedures, the compressive and tensile stress differences were 32.8% at the top and 71.6% at the bottom, respectively. When taking into account the experimental and numerical results, the stress variations were 41.0% and 54.6% at the top and bottom, respectively. In this case, despite the difference between the calculated critical normal stress and the measured stresses having increased safety, the proportion of this difference generates raw material waste. In this comparison, the position of neutral axes is relatively similar among all models.

Figure 10 shows the normal stress measured and analytical and numerical procedures at the strain gauge position of the RG4 beam for a load of 10.08 kN. The slopes of the analytical and numerical results are parallel to each other, different from the experimental results, and show a behaviour similar to the results of normal stresses for RG6. Considering both the experimental and analytical procedures, the discrepancies were 26.6% at the top and 35.5% at the bottom. Regarding the experimental and numerical results, the differences in stress were 32.3% and 21.2% at the top and bottom, respectively. Although the differences were in favour of safety, they should not be overlooked. It is noteworthy that the position of the neutral axes is quite similar among the models in this comparison.

Regarding the results for the RG8 beam, which contains a greater volume of synthetic fibres in its reinforcement, the experimental results corroborate those expected from the analytical model and the numerical model. The distribution of normal stresses along the height of the beam cross-section, in which the reinforcement fibres absorb most of the normal stresses instead of the wood fibres, demonstrates the effectiveness of the reinforcement. It can be observed that the load level of 10.08 kN has a relation of 201% between the tension in the reinforcement and in the wood fibres.

Figure 8 - Stress diagram in the cross-section at 200 mm from the load cell position of the RG8 beam

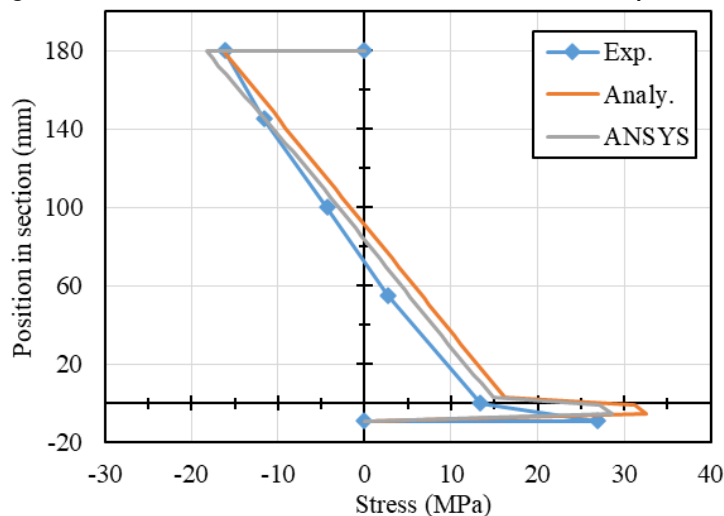


Figure 9 - Stress diagram in the cross-section at 200 mm from the load cell position of the RG6 beam

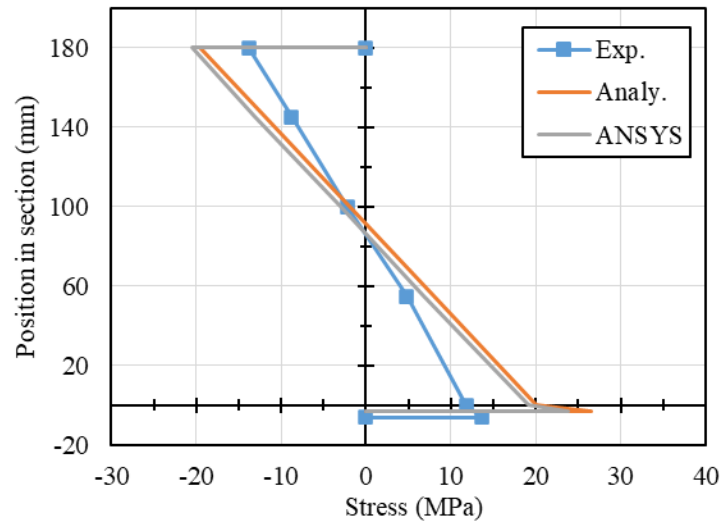
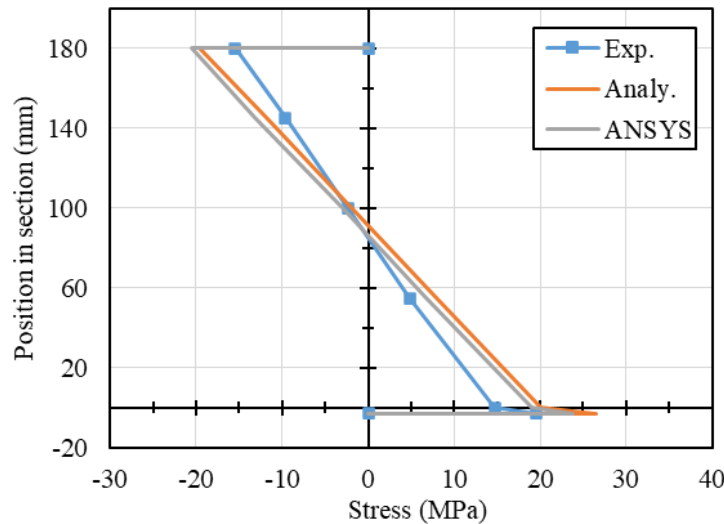


Figure 10 - Stress diagram in the cross-section at 200 mm from the load cell position of the RG4 beam



The disparities observed between the simulated and experimental results of the RG6 and RG4 beams demonstrate significant differences in critical stresses. In this case, using a larger number of specimens is advisable to gain a more in-depth understanding of this issue. A possible explanation for this problem is that it could be associated with the adoption of the mean modulus of elasticity instead of the specific elasticity modulus for each lamination. As the characterization of each lamination was conducted by density, this hypothesis was not tested in this study, but it can be suggested to enhance knowledge on the subject.

Conclusions

This paper aims to analyse the results of vertical displacements and normal stresses by experimental, analytical, and numerical procedures of glulam reinforced with synthetic fibres subjected to bending. These results with unreinforced beams were also compared.

The results indicate that numerical differences between the finite element and transformed section methods are acceptable considering the displacement and normal stresses, both lower than 3%.

The numerical and analytical models are not indicated to initial loads when considering all glued elements between the beams. To have compatibility between the experimental, analytical, and numerical models, the

nonlinearity of fibre reinforcement behaviour due to the initial accommodation of the reinforcement is necessary.

Despite showing improved safety, the normal stresses obtained by the analytical and numerical models were not accurate compared with the normal stresses obtained by the experimental tests.

Based on the results obtained, for the adjustment of analytical and numerical models, in the next stage of the study of the mechanical performance of synthetic Vectran fibres interacting as reinforcement of glulam beams, the behaviour of non-linearity should be evaluated.

References

- ANSYS. **ANSYS workbench products release notes**: ANSYS Workbench Release 19.2. 2018.
- ASSOCIAÇÃO BRASILEIRA DE NORMAS TÉCNICAS. **NBR 7190**: projeto de estruturas de madeira. Rio de Janeiro, 1997.
- BODIG, J.; JAYNE, B. A. **Mechanics of wood and wood composites**. New York: Krieger Pub Co, 1993.
- BORRI, A.; CORRADI, M.; SPERANZINI, E. Reinforcement of wood with natural fibers. **Composites Part B: Engineering**, v. 53, p. 1–8, oct. 2013.
- BRITISH STANDARDS INSTITUTION. **BS EN 1194**: timber structures: glued laminated timber: strength classes and determination of characteristic values. Brussels, 1999.
- CAMPBELL, F. C. **Structural composite materials**. Materials Park: ASM International, 2010.
- DONADON, B. F. *et al.* Experimental investigation of glued-laminated timber beams with Vectran-FRP reinforcement. **Engineering Structures**, v. 202, p. 109818, jan. 2020.
- FIORELLI, J.; DIAS, A. A. Glulam beams reinforced with FRP externally bonded: theoretical and experimental evaluation. **Materials and Structures**, v. 44, n. 8, p. 1431–1440, oct. 2011.
- FRANKLIN INTERNATIONAL. **ReacTITE EP 925 Wood Glue**. Available: <http://www.franklinadhesivesandpolymers.com/Wood-Adhesives-International/Wood-Adhesives/Application/Laminating-Glue/ReacTITE-EP-925.aspx>. Access: 27 feb. 2022.
- GAGNON, S.; PIRVU, C. **CLT Handbook**: cross-laminated timber. Quebec: FPInnovations, 2011.
- GAO, S. *et al.* Mechanical Properties of Glued-Laminated Timber with Different Assembly Patterns. **Advances in Civil Engineering**, v. 2019, ID 9495705, jul. 2019.
- HUANG, H.; TALREJA, R. Effects of void geometry on elastic properties of unidirectional fiber reinforced composites. **Composites Science and Technology**, v. 65, n. 13, p. 1964–1981, oct. 2005.
- İŞLEYEN, Ü. K. *et al.* Behavior of glulam timber beam strengthened with carbon fiber reinforced polymer strip for flexural loading. **Journal of Reinforced Plastics and Composites**, v. 40, n. 17–18, p. 665–685, sep. 2021.
- KURARAY. **Vectran®**: liquid Crystal Polymer Fiber technology: catalog. Available: <http://www.vectranfiber.com/>. Access: 27 feb. 2022.
- MASCIA, N. T.; VANALLI, L. Evaluation of the coefficients of mutual influence of wood through off-axis compression tests. **Construction and Building Materials**, v. 30, p. 522–528, May 2012.
- ONG, C. B. 7 - Glue-laminated timber (Glulam). In: ANSELL, M. P. (ed.). **Wood composites**. Bath: Woodhead Publishing, 2015.
- PEIXOTO, L. S. *et al.* Bending behavior of steel bars reinforced Glulam beams considering the homogenized cross section. **Wood Material Science & Engineering**, p. 1–7, mar. 2021.
- RAFTERY, G. M.; KELLY, F. Basalt FRP rods for reinforcement and repair of timber. **Composites Part B: Engineering**, v. 70, p. 9–19, mar. 2015.
- RESCALVO, F. J. *et al.* Improving ductility and bending features of poplar glued laminated beams by means of embedded carbon material. **Construction and Building Materials**, v. 304, p. 124469, oct. 2021.
- SHAHIDUL ISLAM, M.; SHAHNEWAZ, M.; ALAM, M. S. Glass fiber reinforced Polymer (GFRP) retrofitting of timber I-Joists with opening and notch. **Structures**, v. 34, p. 804–826, dec. 2021.

ŚLIWA-WIECZOREK, K. *et al.* The Influence of CFRP Sheets on the Load-Bearing Capacity of the Glued Laminated Timber Beams under Bending Test. **Materials**, v. 14, n. 14, p. 4019, jan. 2021.

THORHALLSSON, E. R.; HINRIKSSON, G. I.; SNÆBJÖRNSSON, J. T. Strength and stiffness of glulam beams reinforced with glass and basalt fibres. **Composites Part B: Engineering, Composite Lattices and Multiscale Innovative Materials and Structures**, v. 115, p. 300–307, apr. 2017.

TIMBOLMAS, C. *et al.* Transformed-section method applied to multispecies glulam timber beams subjected to pure bending. **Mechanics of Advanced Materials and Structures**, p. 1–10, oct. 2021.

UZEL, M. *et al.* Experimental investigation of flexural behavior of glulam beams reinforced with different bonding surface materials. **Construction and Building Materials**, v. 158, p. 149–163, jan. 2018.

VAHEDIAN, A.; SHRESTHA, R.; CREWS, K. Experimental and analytical investigation on CFRP strengthened glulam laminated timber beams: full-scale experiments. **Composites Part B: Engineering**, v. 164, p. 377–389, 1 May 2019.

WANG, Y. *et al.* The bending-shear behaviors of steel reinforced fast-growing poplar glulam beams with different shear-span ratios. **Construction and Building Materials**, v. 300, ID 124008, sep. 2021.

Acknowledgments

The authors would like to thank the Brazilian Coordination for the Improvement of Higher Education Personnel (CAPES) and National Council for Scientific and Technological Development (CNPq) for the financial support given to enable this work to be carried out.

Ramon Vilela

Conceptualization, Data curation, Formal analysis, Investigation, Methodology, Software, Validation, Writing - original draft, Writing - review & editing.

Faculdade de Engenharia Civil, Arquitetura e Urbanismo | Universidade Estadual de Campinas | Rua Saturnino de Brito, 224 | Campinas - SP - Brasil | CEP 13083-889 | Tel.: (19) 3521-2307 | E-mail: ramonvilela@outlook.com

Nilson Tadeu Mascia

Conceptualization, Formal analysis, Funding acquisition, Investigation, Methodology, Supervision, Writing - original draft, Writing - review & editing.

Faculdade de Engenharia Civil, Arquitetura e Urbanismo | Universidade Estadual de Campinas | E-mail: ntm@unicamp.br

Bruno Fazendeiro Donadon

Conceptualization, Data curation, Formal analysis, Investigation, Methodology.

Faculdade de Engenharia Civil, Arquitetura e Urbanismo | Universidade Estadual de Campinas | E-mail: donadon.bf@gmail.com

Julio Soriano

Formal analysis, Supervision, Writing - review & editing.

Faculdade de Engenharia Agrícola Universidade Estadual de Campinas | Av. Cândido Rondon, 501 | Campinas - SP - Brasil | CEP 13083-875 | Tel.: (19) 3521-1040 | E-mail: julio.soriano@feagri.unicamp.br

Editores do artigo: **Marcelo Henrique Farias de Medeiros** e **Júlio Cesar Molina**

Editor de seção: **Ercília Hitomi Hirota** e **Juliana Parise Baldauf**

Ambiente Construído

Revista da Associação Nacional de Tecnologia do Ambiente Construído

Av. Osvaldo Aranha, 99 - 3º andar, Centro

Porto Alegre - RS - Brasil

CEP 90035-190

Telefone: +55 (51) 3308-4084

www.seer.ufrgs.br/ambienteconstruido

www.scielo.br/ac

E-mail: ambienteconstruido@ufrgs.br



This is an open-access article distributed under the terms of the Creative Commons Attribution License.